Galvanic Corrosion of Strands in Re-Grouted, Post-Tensioned Concrete Bridges

Karthikeyan Manickam and Radhakrishna G. Pillai‡,**

Grouted, post-tensioned (PTD) concrete systems are widely used to construct bridges, typically with an anticipated corrosion-free service life of 100+ y. However, the usage of inadequate grout materials and grouting practices in PTD concrete systems have caused unwanted air voids in ducts, leading to strand/grout/air interface, carbonation of exposed grout layer, and localized corrosion of strands (say, within about 10 y to 20 y). Re-grouting of voids as a tendon repair strategy has led to accelerated galvanic corrosion of the portion of strands at the interface between the carbonated base grout and repair grout with different chemistry, raising concerns and reluctance in re-grouting of voids in tendons. This work focused on understanding and quantifying the galvanic corrosion at the interface of carbonated base grout and repair grout in a re-grouted tendon. The theoretical analysis based on mixed potential theory estimated a galvanic current density of approximately 2 μA/cm^2 and showed that the galvanic coupling can increase the corrosion current density of the prestressing steel in the base grout by about two-fold. The study on prestressed steel in simulated solutions estimated a galvanic current density of approximately 20 μA/cm^2. Then, the study on prestressing steel in grouts and the analytical simulation estimated galvanic current densities around 1.5 μA/cm^2 to 2 μA/cm^2 at 95% external relative humidity (ERH) and 25°C. A model relating the galvanic current density in grouted systems as a function of ERH was developed, which showed an exponential increase in the galvanic corrosion with an increase in ERH. Also, a case study showed that if the tendon anchorage region experiences 95% ERH for about 20 y, sufficient strand corrosion could happen, and structural behavior can change from ductile to brittle nature, which could be a serious concern for structures in the coastal zone.

KEY WORDS: anchorage, carbonation, galvanic corrosion, grout, post-tensioned concrete, strand, tendon

INTRODUCTION

Segmental post-tensioned (PTD) concrete bridges are widely used due to their faster construction time, enhanced aesthetics, and thinner sections. Grouted (bonded) PTD concrete systems are commonly used in constructing such bridges and are typically designed for a corrosion-free service life of 100+ y.[1] However, the usage of inadequate grout materials and grouting practices in PTD concrete systems have caused excessive bleeding of grouts followed by unwanted air voids, leading to strand/grout/air (SGA) interface, carbonation of the exposed grout layer, and localized corrosion of strands (say, within about 10 y to 20 y).[2-3] Bleeding refers to the segregation of water from the cement or binder of the grout mix. Figure 1(a) shows the photo of a corroded and broken tendon anchorage extracted from a 12-y-old PTD concrete bridge.[4] It can be observed that the top strands were severely corroded, whereas the bottom strands were not corroded. The root cause for corrosion was the presence of voids at the top region of the duct, resulting from the use of inadequate grout material.[4] Likewise, Figure 1(b) shows an inadequately grouted PTD anchorage region with the bottom strands embedded inside the grout and top strands exposed to atmospheric humidity, oxygen, and other deleterious elements. Typically, such voids in the anchorage region are filled or re-grouted with cementitious grouts during the tendon repair without treating the SGA interface, as shown in the zoomed-in images of Figure 2. Galvanic corrosion may occur because of the electrochemical incompatibility at the interface, and this work attempted to quantify such galvanic corrosion through experimental and analytical studies.

The remaining paper is arranged as follows. First, a review of the possible corrosion mechanisms at the anchorage region of grouted PTD concrete systems is presented. Then, the bleed and carbonation resistance of three commercially available post-tensioning (PT) grouts are presented. Then, results from experimental and analytical programs assessing the galvanic corrosion in re-grouted PTD concrete systems and its effect on the service life of PTD concrete systems are presented.

1.1 | Review of Possible Corrosion Mechanisms in Post-Tensioned Anchorage Regions

Figure 2 shows the schematic of a segmental PTD concrete bridge constructed with grouted PTD concrete systems. In such systems, the prestressed tendons are encased inside a plastic duct and filled with cementitious grout. The cementitious grout inside the duct maintains a highly alkaline environment around the tendons and protects them from corrosion. The grout also enables some amount of force transfer by surface bonding. Post-Tensioning Institute (PTI) classifies grouts into four classes: (i) class A grouts are made with cement and water, (ii) class B grouts are made with cement, water, and mineral/chemical admixtures, (iii) class C grouts are prepackaged grouts (engineered grout materials plus water), and (iv) class D grouts are special grouts designed by the engineer at the site.[5] Before the early 2000s, class A or B grouts were used as the grouting material for the majority of the PTD concrete

Submitted for publication: October 03, 2023. Revised and accepted: November 23, 2023. Preprint available online: November 30, 2023, https://doi.org/10.5006/4461.
‡ Corresponding author. E-mail: pillai@civil.iitm.ac.in.
* Department of Civil Engineering, Indian Institute of Technology Madras, Chennai, Tamil Nadu, India, 600 036.

ISSN 0010-9312 (print), 1938-159X (online)

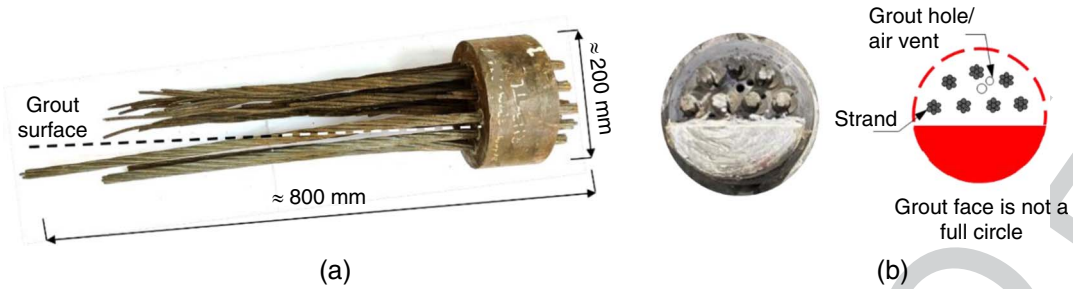

FIGURE 1. *Problems due to inadequate grout materials and grouting practices. (a) Severely corroded and broken tendon anchorage from a 12-y-old bridge and (b) inadequate grouting and sealing of the anchorage in a metro bridge.*

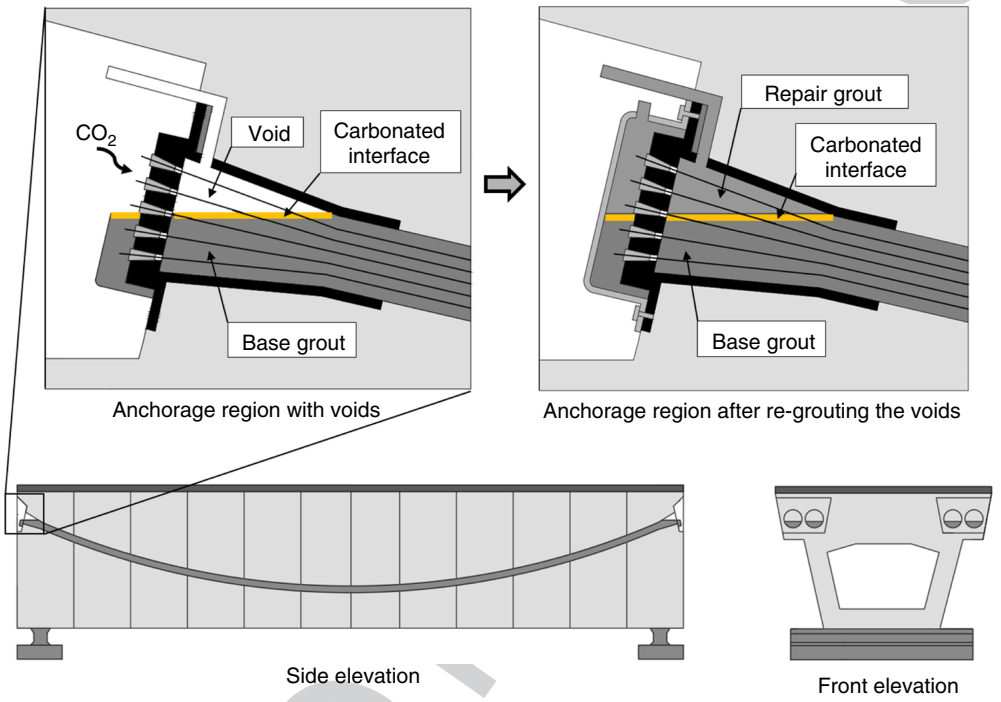

FIGURE 2. *Schematic of a segmental PTD concrete bridge showing the anchorage region before and after re-grouting.*

bridges.[6] These grouts tend to experience a bleed of 3% to 5% by volume, and the bleedwater can rise to the highest points of the ducts.[6-8] Once the bleedwater evaporates or is absorbed into the underlying grout, voids will form near the anchorage region and expose the grout and prestressing steel to humidity, chlorides from air/de-icing salts, and CO_2. Voids due to grout bleed have been extensively reduced after the development of prepackaged thixotropic grouts such as classes C and D grouts. However, these prepackaged grouts may also bleed and segregate sometimes.[9-10] Segregation of grout may lead to deficiencies such as high moisture, high chloride, and high sulfate contents.[11] Also, there can be the formation of pockets of soft grouts. Soft grout represents the situation, where the grout does not harden and remains soft and permeable after setting.[12] These problems in the grout materials can cause variations in pH, density, porosity, and chemical composition of the grouts—creating differences in corrosion potentials to initiate macrocell corrosion.[3] Some of the other possible corrosion mechanisms at the anchorage regions are presented below.

Chlorides could infiltrate the PT duct through the air or from the surface runoff water and accumulate in the void regions. In addition, small amounts of chlorides (>50 ppm) may be present as a part of the original grout.[13] American Concrete Institute recommends the allowable chlorides (acid-soluble) for PT grouts as 0.08% by weight of binder (bwob).[14] Due to the evaporation of bleedwater, the chlorides will settle at hardened grout surfaces (at the SGA interface) and may exceed the threshold limit to initiate corrosion.[15] Studies have reported that corrosion can initiate above a threshold of 0.2% to 0.8% bwob.[16-18] However, there exists a large scatter in the reported values. In addition, the chlorides can act as a catalyst for binding the oxygen atoms to the iron atoms on the steel surface and aggravate the corrosion reactions. Once the chloride has entered the PT duct, the available grout cover is small to prevent the chlorides from reaching the steel, irrespective of the resistance offered by the grout.[19] At the SGA interface, the higher chloride content and lower pH (due to carbonation) substantially elevate the $[Cl^-]/[OH^-]$ ratio compared to the bulk of the grout.[20] This condition can break down the passivity and initiate pitting at the steel surface.[15] Once corrosion initiates at the SGA interface, there will be a galvanic coupling of the relatively small active area (SGA interface) with a larger passive area of the strand embedded in the grout.[15] Chloride exposure for 1 y could reduce the tension capacity of PTD strands by as much as 27%,[21] and failure of strands could likely occur when the local cross-sectional loss reaches 20% to 30%.[22] Apart from

Courtesy: Hansen[28]

FIGURE 3. *Failure of a tendon in a bridge within 4 y after repair (Courtesy: Hansen[28]).*

the chlorides, the segregation of grout could enhance the sulfate content at specific regions (at the SGA interface). Excess sulfate content can reduce the chloride ion binding capacity of the grout.[23] A study reported that the allowable sulfate content of the grout should be limited to 0.07% bwob.[24-25] Therefore, corrosion is determined by the synergistic effects of chloride and sulfate ions.

Generally, cementitious grout consists of 25% to 50% calcium hydroxide and has a pH greater than 13, sufficient to provide an alkaline environment for the passivation of the embedded strand. Upon carbonation, the pH of the grout reduces to 9 or less. The grout in the PT duct of the Mid Bay Bridge in Florida was carbonated to a depth of approximately 6 mm with a pH of approximately 8 after 17 y of construction.[26] Depassivation of strands could occur at the SGA interface due to the carbonation of the grout.[15] In addition to carbonation, the hydrolysis of metal ions further reduces the pH of the grout.[20] Another critical parameter for corrosion is the availability of oxygen, which governs the rate of cathodic reaction. Oxygen is easily available near the anchorage zone compared to the bulk of the duct. The top three to four strands closest to the grout port are mostly affected by corrosion.[17] Such differential aeration processes can aggravate corrosion at the anchorage regions.[27]

In an internal PTD concrete system, tendons are typically concealed within the concrete structure, making it impossible to visually inspect the condition of tendons from the outside. Corrosion of prestressed steel might lower the load-carrying capacity and can result in catastrophic failures if ignored. To address this issue, repairs are necessitated and are performed externally, focusing on the anchorage points. One practical and viable approach for repairing PTD anchorage systems involves re-grouting the voids with cementitious grout. As shown in Figure 2, in many instances, the voids are re-grouted with cementitious grouts (referred to as repair grouts) without treating the underlying issue of the carbonated grout interface. This situation can lead to an electrochemical mismatch at the SGA interface, because of the variations in properties (physical and chemical) of the base grout and the repair grout. This, in turn, can lead to the formation of a corrosion cell. A case study concerning a bridge in Virginia serves as an example of tendon failure induced by galvanic corrosion.[28] The bridge was detected with voids during a regular inspection. To rectify the situation, a repair strategy was implemented, involving the filling of voids with high-performance repair grout. Approximately 4 y later, a tendon failure occurred at the junction of the base grout and repair grout, as shown in Figure 3. The base grout and repair grout exhibited different physical and chemical properties, which led to the development of a macrocouple corrosion. This is a type of galvanic corrosion where the same metal undergoes corrosion due to two dissimilar environments.[13] Lau, et al., investigated this mechanism through laboratory experiments and reported no evidence of significant corrosion development in PTD tendons with voids repaired with dissimilar grout.[3] However, definite conclusions could not be derived from the limited information, and much research is needed to understand the corrosion mechanism, which is the focus of this study.

RESEARCH SIGNIFICANCE

Many developing countries are witnessing a construction boom, and a lot of PTD concrete bridges have been constructed by them, especially during the last two decades. However, a large inventory of such bridges is inadequately grouted due to inadequate grout materials and grouting practices. Also, most of such bridges operate without sufficient protection at the anchorage regions (For example, the absence of permanent steel or plastic anchorage caps, concrete pourbacks, waterproofing layer, etc.). These factors make the anchorage regions susceptible and more vulnerable to corrosion. At present, the majority of such bridges are relatively young (say, about 10 y to 20 y), and they may soon start showing signs of strand corrosion. Repairing such a large inventory of inadequately grouted bridges will be a huge economic challenge for the construction industry. Hence, there is a dire need to assess the feasibility and efficiency of the available repair strategies to prevent/control the corrosion of PTD concrete systems. However, due to difficulties in accessing the tendons of internal PTD concrete bridges, repair techniques such as cable de-humidification, chemical impregnation, re-greasing, etc., may not always be feasible. The most feasible repair solution would be to fill or re-grout the voids with cementitious grouts. Nonetheless, there exists a hesitancy to use cementitious grouts for re-grouting voids because of concerns about possible galvanic corrosion. Hence, there is a need to understand the severity of galvanic corrosion associated with the re-grouting of tendons. This work assessed and quantified the severity of galvanic corrosion using experimental and analytical techniques. A model relating the galvanic current density and external relative humidity (ERH) was developed, which can be used as a tool to estimate the service life of re-grouted PTD concrete systems. The findings will be crucial for repair engineers and decision-makers to develop, plan, and budget repair strategies that will guarantee a target service life of 100+ y for PTD concrete bridges.

MATERIALS AND METHODOLOGY

In this study, three commercially available PT grouts confirming to class A, B, and C specifications as per PTI were tested for their bleed and carbonation resistances.[4] The grouts are (i) plain cement grout (PCG) with a water/binder (w/b)

ratio of 0.44 (class A), (ii) site-batched grout (SBG) with a w/b ratio of 0.45 and plasticized expansive admixture dosage of 0.45% bwob (class B), and (iii) prepackaged grout (PPG-TF) with a w/b ratio of 0.27 (class C). PCG and SBG are conventional PT grouts, while PPG-TF is a new-generation prepackaged thixotropic grout. SBG was/is used for grouting tendons in many developing countries, and hence, it was used in galvanic corrosion experiments. The galvanic corrosion was assessed using the following approaches: (i) theoretical estimate based on mixed potential theory, (ii) prestressed steel in simulated pore solutions with different pH, (iii) prestressing steel in carbonated and pristine grouts, and (iv) simulating the galvanic corrosion using analytical modeling.

3.1 | Bleed and Carbonation Resistance of Post-Tensioning Grouts

Before assessing galvanic corrosion, it was essential to understand the bleed and carbonation resistances of grouts used in PTD concrete bridges. The bleed resistance of PT grouts was assessed using the wick-induced bleed test specified in EN 445:2007.[29] In this test, 900 mL of freshly mixed grout was placed inside a graduated cylinder comprising a 15.2 mm diameter strand. The bleedwater formed at the top surface of the cylinder was measured using a micropipette after 3 h of mixing and was represented in percentage with respect to the initial volume of the grout.

The carbonation resistance of PT grouts was assessed by monitoring the carbonation depth of specimens exposed to an accelerated CO_2 environment (≈3% CO_2, 25±1°C, and ± 65 ±1% ERH). For this, prisms (25 mm × 25 ×mm 285 mm) were cast with all three grouts. After 1 d, the specimens were demolded and coated with three layers of epoxy on all faces except for the top face to facilitate the one-dimensional diffusion of CO_2. After about 1 d of hardening of epoxy, the specimens were kept in a carbonation chamber. The carbonation depth was measured at regular intervals by breaking a thin slice of the specimen perpendicular to the axis and spraying the phenolphthalein indicator solution (1% by weight of indicator mixed in a 70% to 30% blend of ethanol and distilled water). The colorless and pink regions indicate carbonated and pristine grouts, respectively. Furthermore, a pH electrode was used to measure the pH of the grout. Samples were collected from the grout and were ground to a size less than 100 µm. Then, approximately 2 g of ground sample was mixed with 10 mL of de-ionized water and stirred thoroughly on a stirring plate for 30 min. The solution was then allowed to stand for 30 min, and the pH of the solution was measured using a pH electrode.

3.2 | Design of Corrosion Cell for Assessing the Galvanic Corrosion

Figure 2 shows the schematic of a PTD anchorage region before and after re-grouting the voids. Before designing specimens simulating the interface of base and repair grouts, it was essential to understand the expected carbonation depth of grout in PTD concrete bridges. For that, SBG, which was/is commonly used for grouting tendons in PTD bridges, was selected. Prisms (25 mm × 25 mm × 285 mm) were cast with SBG and exposed to a natural sheltered environment. The methodology presented in the *Bleed and Carbonation Resistance of Post-Tensioning Grouts* section was used for the specimen preparation and testing except for the exposure. Figure 4 shows the evolution of carbonation depth in SBG when exposed to a natural sheltered environment. After about 1 y of exposure,

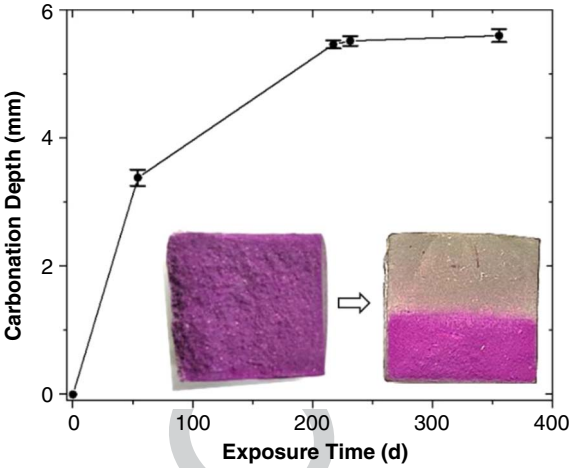

FIGURE 4. *Evolution of natural carbonation depth in site-batched grout.*

a carbonation depth of approximately 6 mm was observed, followed by a flattening in the carbonation depth profile. It was inferred that the rate of increase in carbonation depth would be minimal after this point, and a carbonation depth of 10 mm was assumed to be expected for SBG in PTD concrete bridges. Therefore, grout specimens with a depth of 10 mm were prepared for galvanic corrosion studies.

3.3 | Assessment of Theoretical Galvanic Corrosion Using Mixed Potential Theory

Mixed potential theory was used to assess the theoretical galvanic corrosion. The approach involves superimposing the individual electrochemical responses of the prestressing steels in base and repair grouts, which were determined through potentiodynamic polarization scans (PDS). Figure 5 shows the three-electrode setup and corrosion cell used for the electrochemical impedance spectroscopy (EIS) and PDS with the prestressing steel-grout specimen as the working electrode (WE), nichrome mesh as the counter electrode (CE),

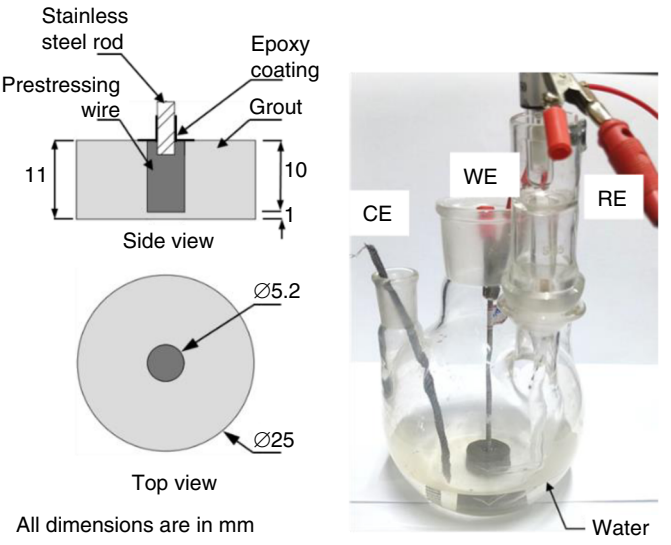

FIGURE 5. *Schematic of the specimen and the photo of the corrosion cell used for EIS and PDS.*

a saturated calomel electrode as the reference electrode (RE), and tap water (with a pH ≈ 8) as the electrolyte. The EIS testing was conducted with an amplitude of ±10 mV and a frequency range from 10^5 Hz to 0.01 Hz at open-circuit potential (OCP). For PDS, the specimens were polarized from −200 mV_{OCP} to +200 mV_{OCP}, with a scan rate of 0.127 mV/s. The specimen was cast with prestressing steel and SBG. After 1 d, the steel specimen was allowed to passivate in a 65±1% ERH and 25±1°C environment for 7 d. Then, the specimen was allowed to depassivate in a carbonation chamber (3% CO_2, 25±1°C, and 65±1% ERH) for about 45 d, which was assessed using EIS. This specimen represents the steel within the carbonated base grout. Similarly, another specimen was cast, demolded after 24 h, and subsequently tested for PDS. This specimen represents the prestressing steel within the pristine repair grout.

3.4 | Quantification of Galvanic Corrosion of Prestressed Steel in Simulated Solutions

The effect of prestress on galvanic corrosion was investigated using a solution study. The galvanic current was measured using prestressed steels exposed to solutions simulating the base grout (simulated carbonated pore solution with a pH of 9, SPS-9) and repair grout (simulated uncontaminated pore solution with a pH of 13, SPS-13), respectively. Table 1 presents the composition of both solutions. Figure 6 shows the dog-bone-type steel specimens used in this study. Typically, dog-bone-type specimens are used in tension tests to eliminate the influence of stress concentrations induced by the loading grips. As shown in Figure 6, the dog-bone-type specimens have shoulders at both ends and a gauge section in between. The shoulders are wider than the gauge section, which enables the stress concentration to occur in the middle when the specimen is loaded with a tensile force. The dog-bone type specimens were extracted from a 5.2 mm diameter king-wire of a 7-wire prestressing strand using an electrical discharge machining process. Openings were made at the top and bottom shoulder portions of the specimens to enable stressing the specimens. The inside of the openings of the specimens was coated with three layers of electrically insulative epoxy to electrically isolate the specimens from the stressing rod. The epoxy was a proprietary product with a high breakdown voltage of 33 kV and a high dielectric strength of 59 kV/mm. The breakdown voltage of an insulator represents a minimum voltage that can cause a portion of the insulator to experience an electrical breakdown and become electrically

Table 1. *Composition of the Simulated Pore Solutions*

Constituents	Concentration (g/L)	
	Simulated Uncontaminated Concrete Pore Solution (SPS-13)	Simulated Carbonated Concrete Pore Solution (SPS-9)
Calcium hydroxide	0.30	0
Sodium hydroxide	10.40	0
Potassium hydroxide	23.23	0
Sodium carbonate	0	8.4
Sodium bicarbonate	0	31.5
Distilled water	Remaining	Remaining

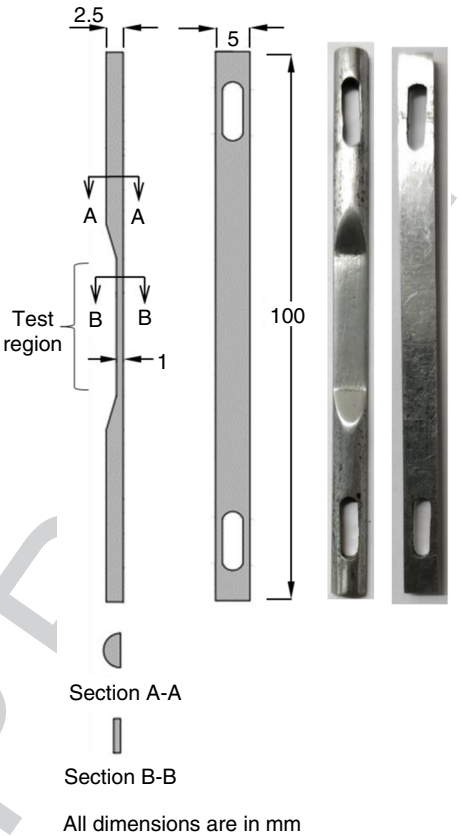

FIGURE 6. *Schematic and photo of the dog-bone-type steel specimen.*

conductive. Similarly, dielectric strength represents the maximum voltage required to produce a dielectric breakdown to allow the flow of charge. A strain gauge (gauge length of 5 mm) was attached to the backside of the specimens before assembling the setup. Then, the specimens were fully coated with three layers of epoxy except for the central gauge region (test region) and the bottom shoulder region (region to establish an electrical connection for galvanic coupling with the other specimen). Figure 7 shows the details of the specimen setup. Self-reacting frames were fabricated and assembled with an in-built corrosion cell with two compartments (say, compartments A and B) and a connecting tube for a salt bridge to establish an ionic connection between the compartments. The prestress was applied manually to the specimens based on the strain measured from the two specimens using the strain gauges. The inner hex nuts on the top side of the reaction frame were screwed outward to impart tension to specimens until the strain corresponding to 50% of the ultimate tensile strength (0.50 f_{pu}) was attained.

Initially, the connecting tube of the corrosion cell was sealed. SPS-13 was filled in compartment A for 7 d to allow the specimen to passivate. The solution was then replaced with SPS-9 and maintained for another 7 d to depassivate the specimen. During this period, compartment B was left unexposed. Then, SPS-9 was removed from compartment A, and the connecting tube was filled with a salt bridge. Generally, salt bridges are used to connect the anodic and cathodic electrolyte solutions of a corrosion cell. In addition, the salt bridge was used to maintain the electrical neutrality of the system by preventing the intermixing of the two electrolytes. In this study,

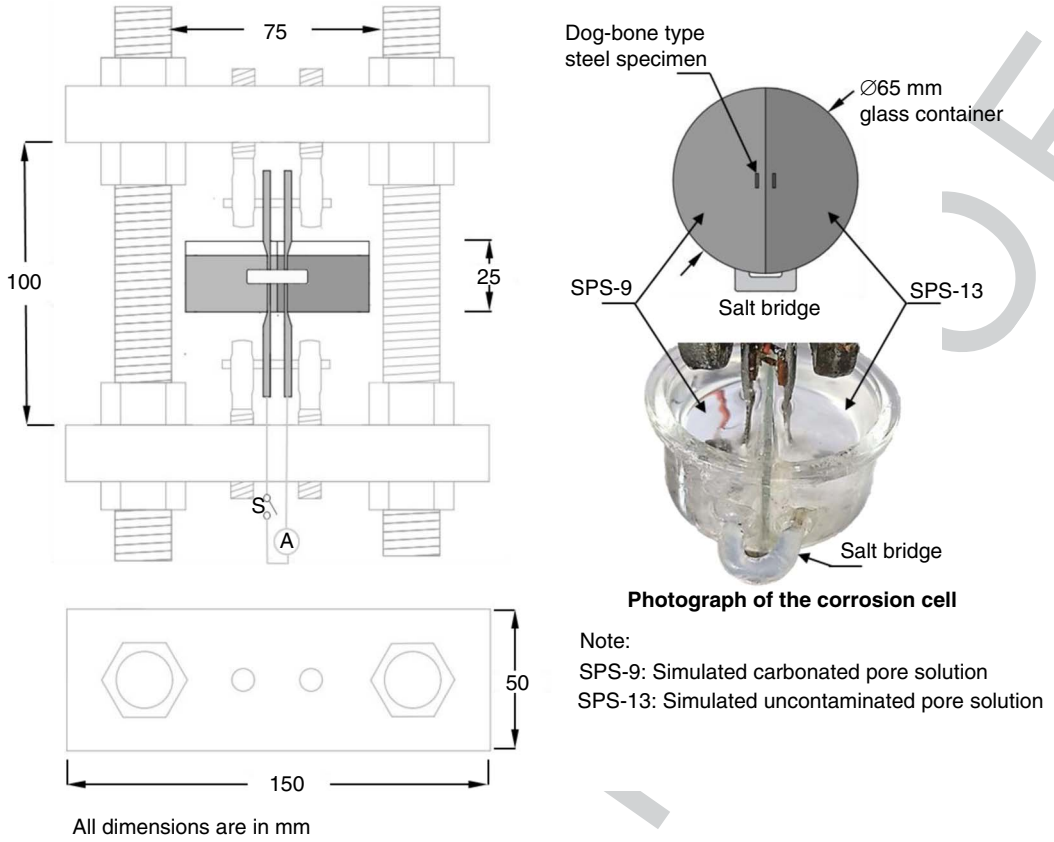

FIGURE 7. *Experimental setup to assess the galvanic corrosion of prestressed steel in simulated solutions.*

nitrate agar was used (5% agar in saturated potassium nitrate solution). Finally, compartment A was again filled with SPS-9, and compartment B was filled with SPS-13. Then, the two specimens were electrically connected, and the galvanic current was measured daily using a pico-ammeter for 30 d.

3.5 | Quantification of Galvanic Corrosion of Prestressing Steel in Grouts

Figure 8 shows details of the specimen designed to replicate a re-grouted tendon. This specimen is divided into two portions, the lower of which represents carbonated base grout and the top, pristine repair grout. The process began with casting the lower portion of the specimen, which included the prestressing steel wire and the base grout (SBG). To passivate the embedded steel, this specimen was kept at 65±1% ERH and 25±1°C for 7 d. Following this, the specimen was carbonated at approximately 3% CO_2, maintained at 25±1°C and 65±1% ERH, for approximately 45 d. The depassivation of the embedded prestressing steel wire was quantified through EIS. Next, the upper portion of the specimen was cast, involving the addition of another prestressing steel wire and a repair grout (SBG). A 1 mm gap was deliberately maintained between the prestressing steels located in the base grout and the repair grout. Subsequently, the prestressing steels were electrically connected and exposed to various levels of eRH (65%, 70%, 75%, 80%, 85%, 90%, and 95%) at a temperature of 25±1°C. Then, the macrocell current was measured using a pico-ammeter.

[†] Trade name.

3.6 | Simulation of Galvanic Corrosion

The galvanic corrosion in re-grouted PTD concrete systems was simulated using the COMSOL Multiphysics®[†] software. For this, a two-dimensional symmetrical geometry replicating the interface of a re-grouted tendon, as shown in Figure 8 but without any gap in between the prestressing steels, was modeled. The governing equations, boundary

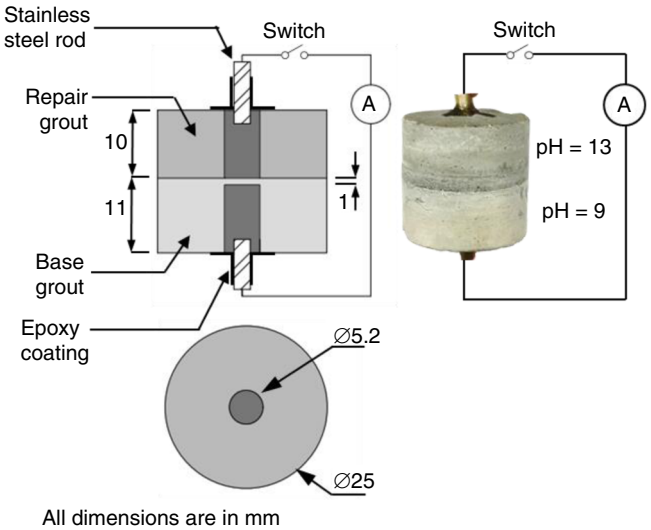

FIGURE 8. *Schematic and photograph of the specimen to quantify galvanic corrosion in grouts.*

conditions, electrode properties, and computed parameters are presented in the *Simulation of Galvanic Corrosion* section.

RESULTS AND DISCUSSIONS

4.1 | Bleed and Carbonation Resistance of Post-Tensioning Grouts

Figure 9 compares the bleedwater volume of three grouts measured after 3 h of grouting. PCG and SBG exhibited a maximum bleedwater volume of approximately 5% and 5.5%, respectively. The inadequate resistance of these grouts to bleeding can be due to the high w/b ratios of the mixes (0.44 and 0.45 for PCG and SBG, respectively). PPG-TF, the prepackaged thixotropic grout showed excellent resistance to bleeding (zero bleedwater volume) due to its low w/b ratio of 0.27. In another work, the authors have extensively studied the performance of various PT grouts, compared the existing specifications, and recommended performance specifications for good grouting materials.[9] As per that study, the recommended that the bleedwater volume of PT grouts be zero to ensure the absence of even a small void. It must be noted that the bleedwater formed in this manner eventually dries up and creates voids in the ducts—exposing the SGA interface and the prestressed steel to humidity and other deleterious elements such as CO_2. Hence, it is also important to understand the resistance of the PT grouts to carbonation, which is presented next.

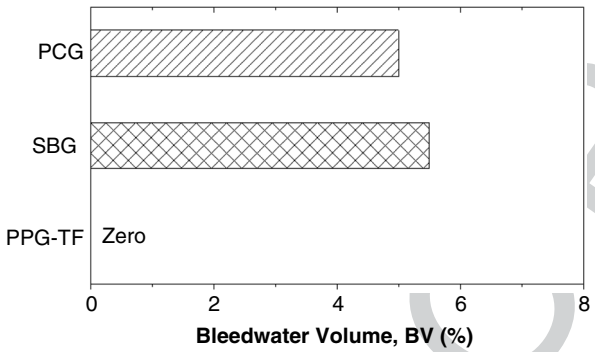

FIGURE 9. *Bleed resistance of PT grouts.*

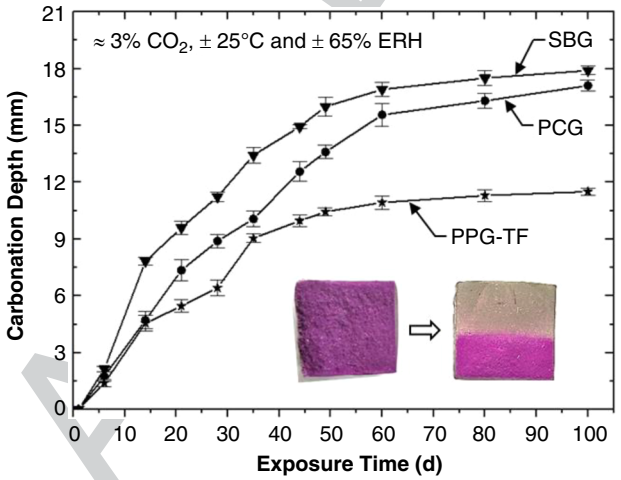

FIGURE 10. *Carbonation resistance of PT grouts.*

Figure 10 compares the evolution of the carbonation depth of three grouts when exposed to an accelerated CO_2 environment. It can be observed that the rate of increase in carbonation was initially fast, and then it started reducing. After 100 d of exposure, SBG and PCG showed inadequate resistance with a carbonation depth of approximately 18 mm and 17 mm, respectively. The poor resistance of these gouts can be correlated to the high w/b ratio of the mixes (0.44 and 0.45 for PCG and SBG, respectively), resulting in a relatively porous microstructure facilitating the diffusion of CO_2. On the contrary, after 100 d, PPG-TF exhibited good resistance with a carbonation depth of approximately 10 mm. The reason for the good resistance can be due to the dense microstructure of the grout due to the low w/b ratio of 0.27.

4.2 | Theoretical Galvanic Corrosion Using Mixed Potential Theory

A mixed potential theory was used to assess the galvanic corrosion at the re-grouted interface. Mixed potential refers to the combined potential of two metals exhibiting different corrosion potentials and electrically connected in the presence of an electrolyte. Potentiodynamic polarization curves can be used to determine the mixed potential and understand the electrode kinetics of two metals in uncoupled and coupled states. For that, PDS was performed on the prestressing steel embedded in the carbonated base grout after 45 d of CO_2 exposure. The depassivation of the embedded prestressing steel upon carbonation was qualitatively assessed using EIS and is presented in the next section. For the prestressing steel embedded in the repair grout, PDS was performed on the specimens after 1 d of casting. Figure 11 shows the superimposed potentiodynamic polarization curves. In the uncoupled state, the prestressing steel in the base grout has an active corrosion potential ($E_{o,BG}$ = −440 mV_{SCE}) with a corrosion current density ($i_{o,BG} \cong 1\ \mu A/cm^2$). At the same time, the prestressing steel in the repair grout has a relatively noble potential ($E_{o,RG}$ = −240 mV_{SCE}) and a corrosion current density ($i_{o,RG} \approx 0.06\ \mu A/cm^2$). The intersection of the anodic branch of the prestressing steel in the base grout and the cathodic branch of the prestressing steel in the repair grout gives the potential and current density of the coupled system. The surface area of the prestressing steels in both grouts was the same (1.84 cm^2);

AQ1

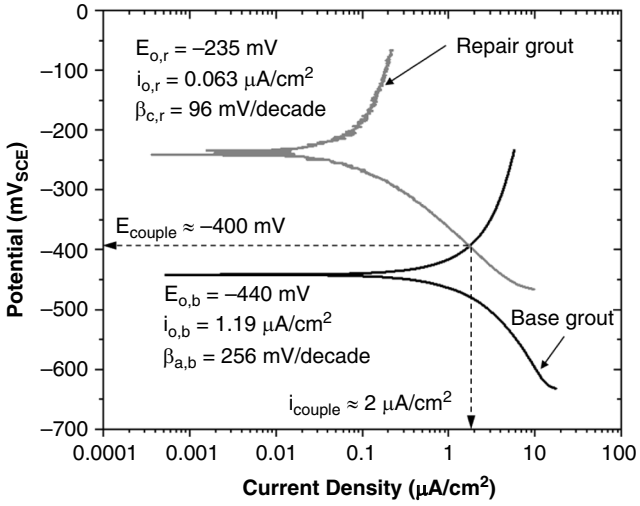

FIGURE 11. *Potentiodynamic polarization curves of the prestressing steels in grouts.*

hence, the resultant mixed potential of the couple occurs at a point, where the total oxidation rate is equal to the total reduction rate. From the superimposed polarization curves, it can be inferred that the mixed potential of the couple is approximately −400 mV_{SCE} with a corrosion current density of approximately 2 $\mu A/cm^2$. It can also be inferred that the galvanic coupling can increase the corrosion current density of the prestressing steel in the base grout from about 1 $\mu A/cm^2$ to 2 $\mu A/cm^2$. In other words, galvanic coupling of the base grout with the repair grout can increase the corrosion current density of the steel in the base grout to about 100%. It has to be emphasized that this estimate is based on theoretical analysis and may not replicate the field conditions. In addition, the areas of the two electrodes in a galvanic couple will influence galvanic corrosion behavior. A greater cathodic area can increase the net galvanic current density, and a greater anodic area can reduce the net galvanic current density. This study assessed the theoretical galvanic current density with the areas of the anode and cathode being the same, and it does not consider the effect of the change in the areas, which is one of the limitations of this study.

4.3 | Assessment of Depassivation of Prestressing Steel upon Carbonation

A qualitative assessment of the depassivation of the prestressing steel embedded in the base grout due to carbonation was made using EIS analysis. Figure 12 shows the typical Nyquist and Bode responses obtained from the tested specimen. These responses reveal the presence of three semicircles with arcs that are incomplete and overlapping. In the inset of Figure 12(a), an equivalent circuit is depicted, which presents three resistors (R) and constant phase elements (Q) in series to represent the response of the specimens. The first semicircle corresponds to the solution (comprising water and grout) and is represented by R_s and Q_s. The second semicircle represents the double layer and is represented by R_{dl} and Q_{dl}. Lastly, the third semicircle signifies the oxide layer (passive layer) formed on the prestressing steel and is represented by R_{ox} and Q_{ox}. The inset of Figure 12(a) also includes a schematic illustrating an ideal EIS response for clarity.

The condition of the passive layer was qualitatively assessed by comparing the characteristics of the oxide layer (R_{ox}). The inclination of the arc in the low-frequency range (10^{-1} Hz to 10^{-2} Hz) within the Nyquist plot provides insight into the condition of the passive layer. A steeper slope indicates a larger-diameter semicircle, signifying a greater R_{ox} value. EIS testing was performed on days 30, 37, and 45 of exposure to carbonation, and a gradual reduction in the slope was observed, indicating the depassivation of the prestressing steel. This depassivation process is evident in the Bode frequency and magnitude plots depicted in Figures 12(b) and (c). There is a gradual decrease in the magnitude at the low-frequency region (0.01 Hz), reflecting alterations in the passive layer. Additionally, $\phi_{0.01}$ decreased from −66° on day 30 to −64° on day 37, and further to −62° on day 45, providing clear confirmation of the depassivation of the specimen. The variations in the electrochemical parameters of the prestressing steel upon carbonation are presented in Table 2.

4.4 | Quantification of Galvanic Corrosion of Prestressed Steel in Simulated Solutions

In this study, the galvanic current was measured between prestressed dog-bone-type specimens immersed in SPS-9 and SPS-13, respectively. The specimens were

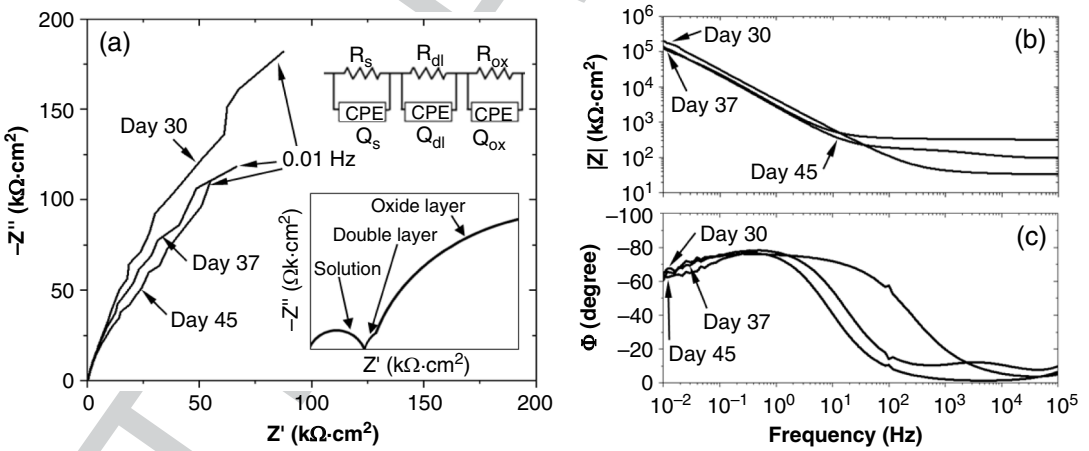

FIGURE 12. *Typical EIS representation used to assess the depassivation of the prestressing steel. (a) Nyquist representation, (b) Bode magnitude, and (c) Bode phase representations.*

Table 2. *Variations in the Electrochemical Parameters of the Prestressing Steel in Grout upon Carbonation*

Days of Exposure to CO_2	R_s ($k\Omega \cdot cm^2$)	R_{dl} ($k\Omega \cdot cm^2$)	R_{ox} ($k\Omega \cdot cm^2$)	Q_{dl} ($mS/s^{n1}/cm^2$)	n1	Q_{ox} ($mS/s^{n2}/cm^2$)	n2	Φ_{max} (degree)	χ^2 ($\times 10^{-3}$)
30	0.03	0.230	922	399	0.91	856	0.74	−76	0.5
37	0.05	0.780	726	127	0.90	845	0.66	−114	0.2
45	0.09	0.876	366	687	0.80	890	0.71	−89	0.1

stressed to 50% of their ultimate tensile strength to consider the effect of prestress in the measurements. The ambient temperature was maintained at 25±1°C. The area of both the specimens in contact with the electrolytes was kept the same (1 cm^2). In the uncoupled state, the specimen in SPS-13 had a relatively noble potential of −180 mV_{SCE}. At the same time, the specimen in the SPS-9 had an active potential of −360 mV_{SCE}. A potential difference/driving voltage of approximately 180 mV existed between the specimens before electrical coupling. Figure 13 shows the measured galvanic corrosion current density. It can be observed that the galvanic current density fluctuates around 20 μA/cm^2 to 25 μA/cm^2 for the first 14 d and then attains a stable value. As per the current direction, the specimen in the SPS-9 is the anode, and the specimen in the SPS-13 is the cathode. At the end of 30 d, the specimens were uncoupled, and the OCP was measured. The OCP of specimens in SPS-13 and SPS-9 was measured as −170 mV_{SCE} and −380 mV_{SCE}, respectively. It can be inferred that the galvanic coupling shifted the OCP of the specimen in SPS-9 toward a more anodic direction from −360 mV_{SCE} to −380 mV_{SCE}, which can be due to the anodic dissolution. At the same time, the OCP of the specimen in SPS-13 was shifted toward a more cathodic direction from −180 mV_{SCE} to −170 mV_{SCE}, which can be due to the possible passivation of the prestressed steel because of the generation of hydroxyl ions associated with the cathodic reaction. It has to be specified that the testing was performed in solutions, and the estimate can be an overestimation of the actual galvanic corrosion. In this study, the areas of the anode and cathode were the same, and it does not consider the effect of the change in the areas, which is one of the limitations of this study.

4.5 | Quantification of Galvanic Corrosion of Prestressing Steel in Grouts

Figure 14 compares the galvanic current densities measured at various ERH. It can be observed that the galvanic current density increases exponentially with an increase in the ERH. The increase in the galvanic current is due to the increase in the ionic conductivity of the grout at higher ERH. According to the direction of the galvanic current, the prestressing steel in the base grout serves as the anode, while the prestressing steel in the repair grout serves as the cathode. A model relating the galvanic current density (i) and the ERH was developed using a weighted regression analysis, as shown in Equation (1). In this analysis, different weights were given to galvanic current

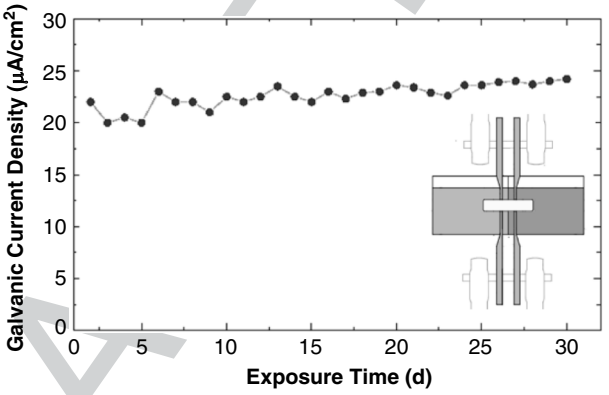

FIGURE 13. *Galvanic current density of prestressed steel in simulated solutions.*

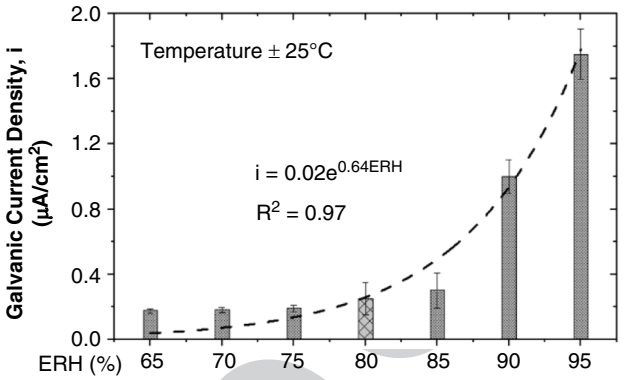

FIGURE 14. *Galvanic current density of prestressing steel in grouts.*

densities at different ERH based on their importance (more weightage for data at ERH 85%, 90%, and 95%).

$$i = 0.02e^{0.64ERH} \quad (1)$$

As per the developed model, it can be inferred that the increase in galvanic current density is not significant between 65% and 85% ERH. However, an exponential increase in the galvanic current density is expected when the ERH increases beyond 85%. This model can be used as a tool to estimate the galvanic current densities for various ERH, which then can be used to estimate the service life of PTD concrete systems, which is presented later in this paper.

4.6 | Simulation of Galvanic Corrosion

The galvanic corrosion in re-grouted PTD concrete systems was simulated using an in-built analytical modeling tool in COMSOL Multiphysics® software. A two-dimensional symmetrical geometry replicating the interface, of the base grout and repair grout, as shown in Figure 8, but without any gap in between the prestressing steels was created. The prestressing steel in the base grout was assumed to be the anode, and the prestressing steel in the repair grout was assumed to be the cathode. The boundary of the electrodes was surrounded by grouts with conductivities of σ_1 (base grout) and σ_2 (repair grout). Stagnant electrolytes were assumed, and hence Laplace equation was used as the governing equation as given in Equation (2). The numerical solution to the Laplace equation requires the definition of the electrochemical parameters of the anode, cathode, and electrolytes, which were determined using PDS and EIS. The Tafel expression given in Equation (3) was used to analyze electrode kinetics

$$\nabla^2 \varphi = 0 \quad (2)$$

$$\Delta V = \beta \times \ln(i=i_o) \quad (3)$$

where φ is the electrochemical potential, ΔV is the overpotential (V), β is the Tafel slope (mV/decade), i is the current density (A/cm^2), and i_o is the exchange current density (A/cm^2).

A secondary current distribution interface was selected under the corrosion module tool to account for the activation overpotential. A time-dependent initialization interface was used to incorporate deformed mesh physics in the model. The study is completed in two steps. The first step comprises a current distribution initialization that resolves only potential fields, and in the second step, potential fields computed in the

Table 3. *Electrode and Electrolyte Parameters for Simulating the Galvanic Corrosion*

Parameter	Value
Free corrosion potential of steel in the base grout, $E_{o,BG}$ (mV_{SCE})	–440
Free corrosion potential of steel in the repair grout, $E_{o,RG}$ (mV_{SCE})	–230
Exchange current density of steel in the base grout, $i_{o,BG}$ ($\mu A/cm^2$)	1.19
Exchange current density of steel in the repair grout, $i_{o,RG}$ ($\mu A/cm^2$)	0.063
Anodic Tafel slope of steel in the base grout, $\beta_{a,BG}$ (mV/decade)	256
Cathodic Tafel slope of steel in the repair grout, $\beta_{c,RG}$ (mV/decade)	96
Conductivity of the base grout, σBG (μS/m)	2.7
Conductivity of the repair grout, σRG (μS/m)	8.6

first step are used as initial values in a time-dependent study. Figure 11 presents the polarization curves of the prestressing steels in the base grout and the repair grout, respectively. The electrode and electrolyte parameters are presented in Table 3. The conductivity of the base grout and repair grout was determined from EIS. Figure 15 shows the Nyquist representation of the EIS responses of the grout specimens. The average electrical conductivities of the base grout and the repair grout were determined as 2.7 μS/m and 8.6 μS/m, respectively.

The galvanic corrosion was assessed using the electrode current density and total electrode thickness change. Figure 16 shows the computed corrosion parameters. Figure 16(a) shows the current density distribution, which is important while analyzing the extent of galvanic corrosion that has taken place at the electrode/electrolyte interface. From the computed electrode current density, it can be observed that the junction area was the most affected region with a magnitude of 2 $\mu A/cm^2$. The current density was most severe near the interface, and then a constant current density was observed as moving away from the interface. The total electrode thickness change is represented by the different color distributions in Figures 16(b) and (c). The prestressing steel at the interface is the most affected region, and the degradation was shown clearly in the zoomed image. At the end of 24 h, a metal layer of 0.05 μm has been degraded from the interface. The dark blue region represents the maximum thickness change, and the value lies around 200 μm at the end of 20 y. The electrode thickness change was most severe near the interface, and then a constant thickness change (50 μm) was observed as moving away from the interface.

4.7 | Effect of Galvanic Corrosion on the Service Life of Post-Tensioned Concrete Systems

Figure 17 compares the galvanic current densities assessed from different approaches. The theoretical analysis based on mixed potential theory estimated a galvanic current density of approximately 2 $\mu A/cm^2$. Then, the study on prestressed steel in simulated solutions considering the effect of stress estimated a current density of approximately 20 $\mu A/cm^2$. This estimate can be an overestimation, as the test was conducted in solutions and resistivity of the grout was not considered. Then, the experimental program on the prestressing steel in grouts estimated a galvanic current density of approximately 1.7 $\mu A/cm^2$ at 95±1% ERH and 25±1°C. Then, the results from the analytical modeling estimated a galvanic current density of approximately 2 $\mu A/cm^2$ at the interface of the base grout and repair grout at 95±1% ERH and 25±1°C. The estimates from theoretical analysis, prestressing steel-grout study and the analytical modeling have agreed well with each other.

To understand the severity of galvanic corrosion on the service life, a case study assuming a PTD bridge situated in a coastal environment with an ambient temperature of ±25°C throughout the year was considered. A 5% loss in mass due to corrosion was assumed to be the limit state to change the behavior of the PTD tendon system from ductile to brittle. The galvanic current densities from the study on prestressing steel in grouts at different ERH were considered in the analysis to estimate the theoretical mass loss. Faraday's law of electrolysis was used to estimate the theoretical mass loss. The analysis showed that ductile to brittle transition could happen at 95 y, 35 y, and 20 y if a structure experiences galvanic current densities of 0.65 $\mu A/cm^2$, 1 $\mu A/cm^2$, and 1.7 $\mu A/cm^2$, respectively, which were the estimated galvanic current densities at 85%, 90%, and 95% ERH. Hence, this study emphasizes the severity of the possible galvanic corrosion at the interface of grouts in a re-grouted PTD tendon.

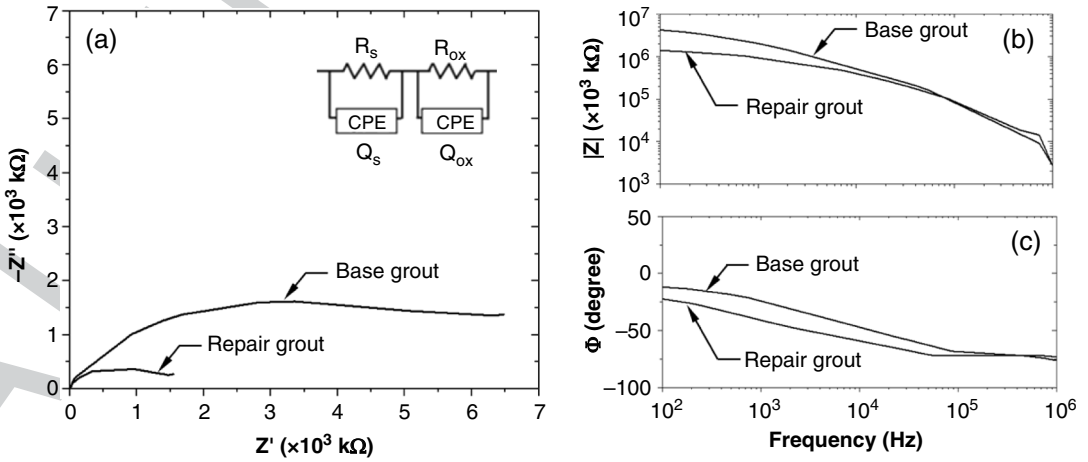

AQ3 **FIGURE 15.** *Typical EIS response used to calculate the conductivity of grouts.*

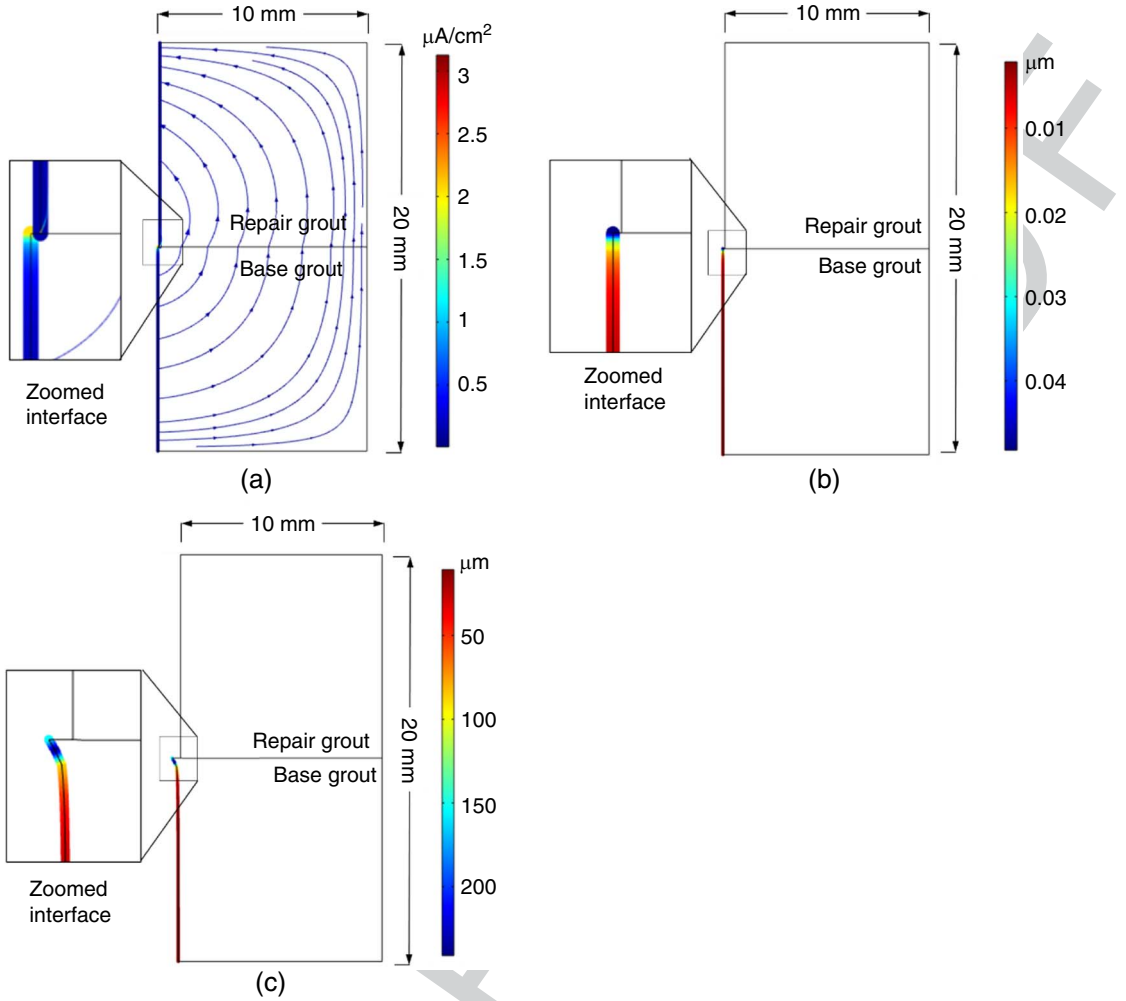

FIGURE 16. *Computed corrosion parameters. (a) Current density distribution at 1 d, (b) electrode thickness loss at 1 d, and (c) electrode thickness loss at 20 y.*

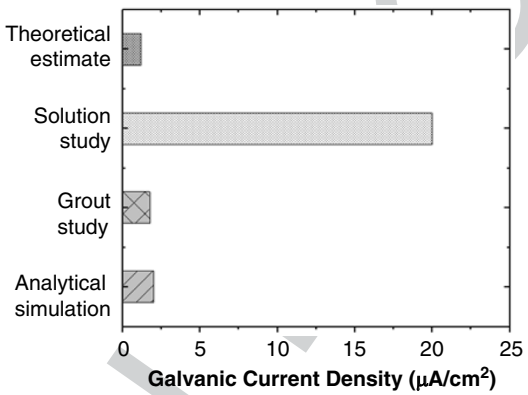

FIGURE 17. *Comparison of the galvanic current densities.*

CONCLUSIONS

➢ Significant void and consequent strand corrosion have been observed in various grouted PTD concrete systems. Even re-grouting tendons has not shown to be very effective in many instances. In this study, the galvanic corrosion of the portion of strands at the interface between the carbonated base grout and repair grout in a re-grouted tendon was assessed using experimental and analytical methods. The following are the major conclusions drawn.

➢ The PCG and SBG exhibited inadequate bleed and carbonation resistance because of their high w/b ratios; hence, they are not recommended for use as PT grouts. On the other hand, the commercially available prepackaged thixotropic grout (PPG-TF) exhibited excellent bleed and carbonation resistance. Hence, PPG-TF is recommended for use as PT grouts to prevent the formation of voids and associated corrosion in PTD concrete systems.

➢ The study on prestressed steel in simulated solutions using dog-bone-shaped specimens estimated a galvanic current density of approximately 20 μA/cm^2 at 25±1°C. However, this value can be an overestimation, as the specimens were tested in simulated solutions, and the resistivity of the grout was not considered.

➢ The theoretical analysis of galvanic corrosion using the mixed potential theory (Evan's diagram) estimated a galvanic current density of approximately 2 μA/cm^2. It was inferred that the galvanic coupling of the prestressing steel in the base grout with the prestressing steel in the repair grout can increase the galvanic corrosion of the prestressing steel in the base grout two-fold.

➢ The study on prestressing steel in grouts estimated a galvanic current density of approximately 1.7 μA/cm^2 at 95±1%

ERH and 25±1°C. A model relating the galvanic current density (i) and the ERH was developed as follows: $i = 0.02e^{0.64ERH}$. The analytical simulation estimated a galvanic current density of approximately 2 μA/cm^2 at 95±1% ERH and 25±1°C. It was inferred that galvanic corrosion would be more severe at or near the interface of the base grout and repair grout, highlighting the possibility of strand breakages and catastrophic failures much before the target design service life. The analytical simulation agreed well with the theoretical estimate and the study on prestressing steel in grouts. Also, a case study showed that if the tendon anchorage region experiences 95% ERH for about 20 y, sufficient strand corrosion could happen, and structural behavior can change from ductile to brittle nature, which could be a serious concern for structures in the coastal zone.

➢ These results highlight the severity of possible galvanic corrosion in re-grouted PTD concrete systems. Therefore, it is necessary to develop appropriate preventive maintenance strategies that will guarantee a target service life of 100+ y for PTD concrete bridges. The problem could be controlled by restoring the pH of the carbonated interface before re-grouting the tendons. Electrochemical treatment such as galvanic anode cathodic protection can be used to protect the anchorage system.

ACKNOWLEDGMENTS

The authors acknowledge the financial support through the Centre of Excellence on Technologies for Low Carbon and Lean Construction at the Indian Institute of Technology Madras (IITM), Chennai, India, with the support of the Ministry of Education of the Government of India. The financial support for the first author by the Ministry of Education of the Government of India is acknowledged. The authors thank Prof. Lakshman Neelakantan from IITM for his technical guidance. The authors also acknowledge the testing facility in the Construction Materials Research Laboratory at the Department of Civil Engineering at IITM.

References

AQ4
1. S.B. Im, S. Hurlebaus, D. Trejo, *Transp. Res. Rec.* (2010): p. 3-10.
2. D. Whitmore, I. Lasa, *MATEC Web Conf.* 199 (2018): p. 1-6.
3. K. Lau, I. Lasa, M. Paredes, "Corrosion Failure of Post-Tensioned Tendons in Presence of Deficient Grout," CORROSION 2013, paper no. 2600 (Houston, TX: NACE International, 2013).
4. K. Manickam, R.G. Pillai, *MATEC Web Conf.* 378 (2023): p. 07002.
5. PTI M55.1-12, "Specification for Grouting of Post-Tensioned AQ5 Structures" (Arizona: Post-Tensioning Institute, 2013).
6. ASBI Report, "American Segmental Bridge Institute Grouting Committee: Interim Statement on Grouting Practices" (Arizona: American Segmental Bridge Institute, 2000).
7. S. Kamalakannan, R. Thirunavukkarasu, R.G. Pillai, M. Santhanam, *Constr. Build. Mater.* 180 (2018): p. 681-691.
8. M.K. Mohan, R.G. Pillai, M. Santhanam, R. Gettu, *Constr. Build. Mater.* 281 (2021): p. 122612.
9. K. Manickam, R.G. Pillai, *Indian Concr. J.* 97 (2023): p. 6-20.
10. D. Trejo, M.B.D. Hueste, P. Gardoni, R.G. Pillai, K. Reinschmidt, S.B. Im, S. Kataria, S. Hurlebaus, "Effect of Voids in Grouted, Post-Tensioned Concrete Bridge Construction: Volume 2—Inspection, Repair, Materials, and Risks," report no. FHWA Publ. No. FHWA/TX-09/0-4588-1 Vol. 2, 2009.
11. M.K. Mohan, S. Manohar, R.G. Pillai, M. Santhanam, R. Gettu, *Constr. Build. Mater.* 368 (2023): p. 130345.
12. K.K. Vigneshwaran, S. Permeh, M. Echeverría, K. Lau, I. Lasa, *Corrosion* 74 (2018): p. 362-371.
13. D. Whitmore, T. Arnesen, "Evaluation and Mitigation of Post-Tensioned Steel Corrosion," in *Forensic Engineering: Forging Forensic Frontiers* (ASCE, 2018), p. 879-892. AQ6
14. ACI PRC-222-19, "Guide to Protection of Metals in Concrete Against Corrosion" (Farmington Hills, MI: American Concrete Institute, 2019).
15. A.A. Sagüés, A H. Wang, R.G. Powers, "Corrosion of the Strand-Anchorage System in Post-Tensioned Grouted Assemblies," CORROSION 2003, paper no. 05266 (Houston, TX: NACE International, 2003).
16. S.K. Lee, J. Zielske, "An FHWA Special Study: Post-Tensioning Tendon Grout Chloride Thresholds," report no. FHWA Publ. No. FHWA-HRT-14-039, 2014.
17. R.A. Reis, "Corrosion Evaluation and Tensile Results of Selected Post-Tensioning Strands at the SFOBB Skyway Seismic Replacement Project," California Department of Transportation, 2007. AQ7
18. D. Joseline, R.G. Pillai, L. Neelakantan, *Corrosion* 77 (2021): p. 906-922.
19. Y. Yong-Sik, R. Hwa-Sung, L. Hee-Seob, K. Kyung-Taek, K. Jeong-Su, K. Seung-Jun, *Constr. Build. Mater.* 186 (2018): p. 1005-1015.
20. R.G. Powers, A.A. Sagues, Y.P. Virmani, "Corrosion of Post-Tensioned Tendons in Florida Bridges," report no. FDOT Publ. No. FL/DOT/SMO/04-475, 2016.
21. D. Trejo, R.G. Pillai, M.B.D. Hueste, K.F. Reinschmidt, P. Gardoni, *ACI Mater. J.* (2009): p. 144. AQ8
22. R. Betti, A.C. West, G. Vermaas, Y. Cao, *J. Build. Eng.* 10 (2005): p. 151-162.
23. S. Permeh, K.K. Vigneshwaran, M. Echeverría, K. Lau, I. Lasa, *Corrosion* 74 (2018): p. 457-467.
24. S. Permeh, K.K. Vigneshwaran, K. Lau, I. Lasa, *Corrosion* 75 (2019): p. 848-864.
25. F. Li, X. Luo, Z. Liu, *Struct. Concr.* 18 (2017): p. 902-913.
26. D. Trejo, M.B.D. Hueste, P. Gardoni, R.G. Pillai, K. Reinschmidt, S.B. Im, S. Kataria, S. Hurlebaus, M. Gamble, T.T. Ngo, "Effect of Voids in Grouted, Post-Tensioned Concrete Bridge Construction: Volume 1—Electrochemical Testing and Reliability Assessment," report no. FHWA Publ. No. FHWA/TX-09/0-4588-1 Vol. 1, 2009.
27. M. Carsana, L. Bertolini, *Struct. Infrastruct. Eng.* 11 (2015): p. 402-411.
28. B. Hansen, "Forensic Engineering: Tendon Failure Raises Questions About Grout in Post-Tensioned Bridges," *Civ. Eng. News* (2007), p. 17-18. AQ9
29. EN 445, "Grout for Prestressing Tendons—Test Methods" (*Belgium: European Standard*, 2007).

NOMENCLATURE

PTD	Post-tensioned
PT	Post-tensioning
PCG	Plain cement grout
SBG	Site-batched grout
SGA	Strand-grout-air
SPS	Simulated uncontaminated concrete pore solution
SCPS	Simulated carbonated concrete pore solution
OCP	Open-circuit potential
SCE	Saturated calomel reference electrode
EIS	Electrochemical impedance spectroscopy
PDS	Potentiodynamic polarization scan
bwob	by weight of binder
ERH	External relative humidity
w/b	water to binder ratio
f_{pu}	Ultimate tensile strength

Queries

AQ1: Please mention which section is referred here.
AQ2: Please define the CPE used in the artwork of Figures 12 and 15.
AQ3: Please provide the part label description in Figure 15.
AQ4: Please provide the volume number for reference 1.
AQ5: Please provide the city of publication for references 5,6,29.
AQ6: Please provide the publication city, state or country of publication for reference 31.
AQ7: Please provide the complete details for reference 17.
AQ8: Please provide the volume number for reference 21.
AQ9: Please provide the complete details for reference 28.